Nitrosyl−Heme Structures of *Bacillus subtilis* Nitric Oxide Synthase Have Implications for Understanding Substrate Oxidation[†,‡]

Kartikeya Pant and Brian R. Crane*

Department of Chemistry and Chemical Biology, Cornell University, Ithaca, New York 14853

Received September 15, 2005; Revised Manuscript Received December 23, 2005

ABSTRACT: The crystal structures of nitrosyl−heme complexes of a prokaryotic nitric oxide synthase (NOS) from *Bacillus subtilis* (bsNOS) reveal changes in active-site hydrogen bonding in the presence of the intermediate N^{ω}-hydroxy-L-arginine (NOHA) compared to the substrate L-arginine (L-Arg). Correlating with a Val-to-Ile residue substitution in the bsNOS heme pocket, the Fe(II)−NO complex with both L-Arg and NOHA is more bent than the Fe(II)−NO, L-Arg complex of mammalian eNOS [Li, H., Raman, C. S., Martasek, P., Masters, B. S. S., and Poulos, T. L. (2001) *Biochemistry 40*, 5399−5406]. Structures of the Fe(III)−NO complex with NOHA show a nearly linear nitrosyl group, and in one subunit, partial nitrosation of bound NOHA. In the Fe(II)−NO complexes, the protonated NOHA N^{ω} atom forms a short hydrogen bond with the heme-coordinated NO nitrogen, but active-site water molecules are out of hydrogen bonding range with the distal NO oxygen. In contrast, the L-Arg guanidinium interacts more weakly and equally with both NO atoms, and an active-site water molecule hydrogen bonds to the distal NO oxygen. This difference in hydrogen bonding to the nitrosyl group by the two substrates indicates that interactions provided by NOHA may preferentially stabilize an electrophilic peroxo-heme intermediate in the second step of NOS catalysis.

Nitric oxide synthases (NOS) react with L-arginine (L-Arg)[1] and oxygen to form nitric oxide and citrulline in a two-step reaction that generates N^{ω}-hydroxy L-arginine (NOHA) as a stable intermediate (Figure 1) (*1*−*11*). Conversion of L-Arg to NOHA likely proceeds as a cytochrome P-450-type monooxygenation with the additional NOS cofactor, tetrahydrobiopterin (H_4B) donating an electron to the heme during oxygen activation (*12*, *13*). A compound-I-type species (VI) likely acts in this first oxidation, but a hydroperoxy or peroxy species (V) is proposed to act in the second step (Figure 1) (*3*, *7*, *10*, *14*−*17*). Whether the NOS active center actually carries out the two reactions with different activated oxygen species is an unresolved issue. Product NO can either diffuse out of the heme pocket or bind to the heme iron and inhibit the enzyme (Figure 2) (*15*, *18*, *19*). The three mammalian NOS isozymes bind and release NO to varying degrees; this impacts the delivery of NO as a signaling agent and the generation of oxidized nitric oxide species (*18*−*20*).

Diatomic ligands such as NO, CO, CN^-, and even O_2 have been used to probe NOS active center properties. A recent review by Rousseau and co-workers summarizes our current understanding of these complexes through spectroscopic investigations (*15*). Because of their instability, catalytically key oxy-heme complexes are difficult to trap in crystals; thus, nitrosyl complexes have served as oxygen mimics for structural studies of ternary complexes in heme centers (*15*, *21*). In particular, crystal structures of the nitrosyl−heme complex of bovine eNOS, as well as a cyanide complex of iNOS, provide insight into structures of a ternary precatalytic configuration (*22*, *23*). A model has also been derived for the oxy-heme NOHA ternary species based on the structure of murine iNOS bound to NOHA (*24*).

For both steps of NOS catalysis, low-temperature EPR and ENDOR studies of heme-oxy-L-Arg complexes indicate the involvement of a [guanidium-H_2O] network in the proton-coupled electron transfers that activate oxygen (*25*). In fact, ferrous oxy-heme complexes with either L-Arg or NOHA behave equivalently in cryo-reduction and annealing (*24*, *25*). Both experiments resolve a peroxo-ferric heme species that converts directly to products on raising temperature. Either L-Arg or NOHA could donate protons to heme-bound oxygen in these processes, although the pK_a of NOHA is substantially lower than that of L-Arg (*26*). Crystallographic information on ternary complexes with NOHA may help clarify the structural features that distinguish the two steps of NOS catalysis.

Herein, we report crystal structures of complexes among substrates and nitrosyl−heme (Fe(II)−NO and Fe(III)−NO) species in the prokaryotic NOS protein from *B. subtilis* (bsNOS). Prokaryotic NOSs lack a reductase domain and N-terminal regions found in mammalian NOSs (mNOSs) but have very similar heme environments and catalytic properties compared to mNOSs (*27*−*30*). Close interactions between the substrate and heme-bound NO are characteristic of all structures. In particular, in one structure, we observe partial

[†] This work supported by the National Science Foundation (MCB-0133564) and the Petroleum Research Fund.

[‡] Protein Data Bank coordinate deposition: L-Arg Fe(II)−NO, 2FC1; NOHA Fe(II)−NO, 2FBZ; L-Arg Fe(III)−NO, 2FC2.

* To whom correspondence should be addressed. Telephone: 607-254-8634. Fax: 607-255-1248. E-mail: bc69@cornell.edu.

[1] Abbreviations: L-Arg, L-arginine; NOS, nitric oxide synthase; bsNOS, *Bacillus subtilis* NOS; NOHA, N^{ω}-hydroxy-L-arginine; DFT, density functional theory, Fe(III)−NO, ferric heme−nitric oxide complex; Fe(II)−NO, ferrous heme−nitric oxide complex; ENDOR, electron−nuclear double resonance; ESR, electron-spin resonance.

10.1021/bi0518848 CCC: $33.50
Published on Web 02/04/2006

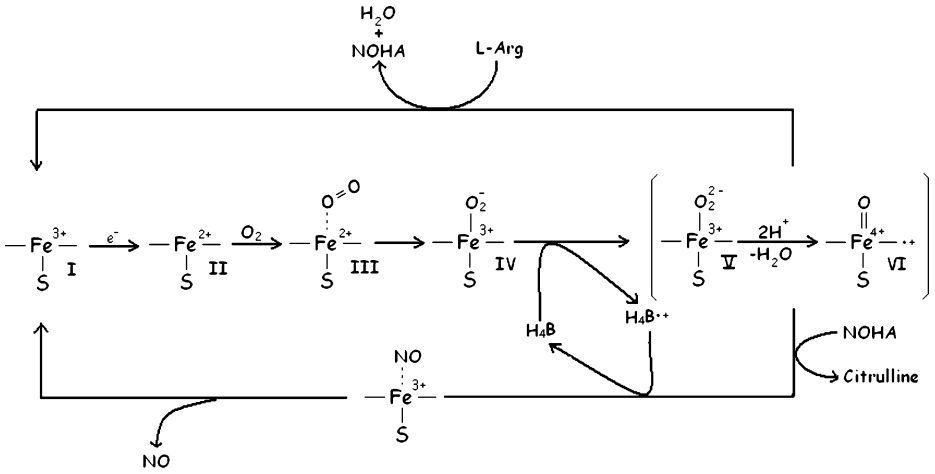

FIGURE 1: The NOS catalytic mechanism. The ferric enzyme (I) is first reduced to the ferrous state (II), which then binds to O_2 (III) to form a ferric superoxide species (IV). An additional electron is added, which leads to the formation of a peroxy species (V). V is proposed to convert to a ferryl compound I species (VI), which inserts an oxygen atom in L-Arg to produce NOHA. In the second step of the reaction, peroxo-heme may serve as the activated oxygen species to catalyze citrulline and NO formation from NOHA. Product NO can either leave the heme pocket or bind to the heme and inhibit the enzyme.

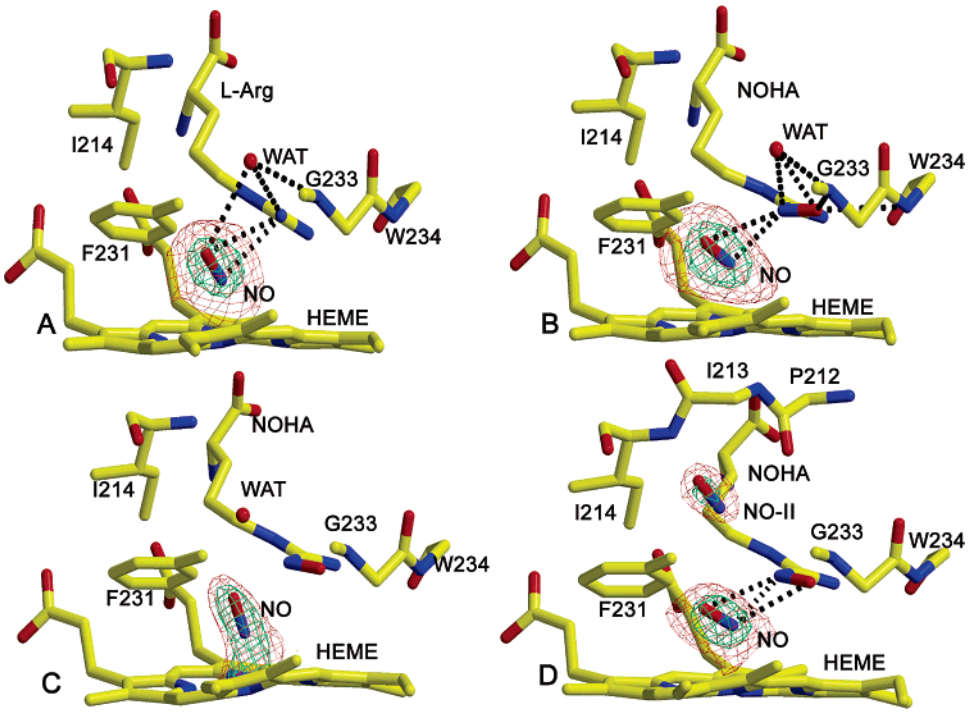

FIGURE 2: bsNOS nitrosyl−heme, substrate complexes. Hydrogen-bonding interactions (<3.3 Å) are shown as dotted lines. (A) Fe(II)−NO-L-Arg complex (3σ and 1σ contours in an $F_o - F_c$ omit map). (B) Fe(II)−NO−NOHA complex (4σ and 1σ contours). The active-site water does not hydrogen bond to the distal NO oxygen, but NOHA hydrogen bonds to the proximal NO nitrogen. (C) The linear Fe(III)−NO−NOHA complex (3σ and 2σ contours). (D) The unusual Fe(III)−NO−NOHA complex (4σ and 2σ contours). A putative second NO molecule (NO−II) is observed in a hydrophobic pocket surrounded by Ile214, Pro212, and Phe231.

nitrosation of the hydroxylated NOHA nitrogen (N^{ω}). Importantly, hydrogen bonding of the NO proximal N with the protonated NOHA N^{ω} produces bent Fe−NO complexes. A similar interaction with heme-bound oxygen may stabilize a peroxo species in the second step of the reaction.

MATERIALS AND METHODS

NOC-12 and dihydrobiopterin were purchased from Alexis and Cayman chemicals, respectively. Poly(ethylene glycol) was obtained from Hampton Research and Tris (hydroxymethyl)aminomethane buffer was from Fisher Scientific. All other chemicals were from Sigma-Aldrich unless otherwise noted.

Protein Expression, Purification, Crystallization and Structure Determination. bsNOS was cloned, expressed, and purified as previously reported (*27*). Initial bsNOS crystals were grown at room temperature by hanging-drop vapor diffusion from 45 mg/mL protein in 50 mM Tris (pH 7.5), 150 mM NaCl, and 2mM DTT that was mixed 1:1 (V/V) with a reservoir solution containing 100 mM sodium cacodylate (pH 6.0−8.0), 200 mM potassium acetate, and 16−21% poly(ethylene glycol) (PEG) 8K (*27*). To generate Fe(II)−NO complexes, crystals were anaerobically grown from seeds in sitting drop solutions containing the same reservoir solution, except 3−8% PEG 8K and 1 mM dihydrobiopterin, 5 mM L-Arg, NOHA or citrulline and 1−20

Table 1: Data Collection and Refinement Statistics of bsNOS Nitrosyl−Heme Complexes in Space Group $P2_12_12$

	Fe(II)−NO + L-Arg	Fe(II)−NO + NOHA	Fe(III)−NO + NOHA
cell *a*, *b*, *c* (Å)	80.0, 93.5, 62.8	80.0, 93.5, 62.8	81.3, 93.2, 118.3
no. of residues	362	362	724
cofactors and ligands	NO, L-Arg, H_2B	NO, NOHA, H_2B	NO, NOHA, H_2B
no. of waters	459	307	738
resolution (Å)	1.9 (1.97−1.9)	1.93 (1.97−1.93)	2.2 (2.25−2.2)
wavelength (Å)	1.100	1.100	0.979
no. of unique reflections	34535	35595	43748
no. of observations	116133	125963	137697
% completeness	91.1 (88.3)	93.9 (92.1)	92.5 (90.4)
$\langle I/\sigma I\rangle$	32.2 (8.6)	8.29 (2.36)	6.24 (3.0)
R_{sym} (%)[a]	0.069 (0.34)	0.117 (0.55)	0.093 (0.235)
R (%)[b]	23.4	23.0	25.9
R_{free}	25.9	25.0	27.3
overall $\langle B\rangle$ (Å^2)	35.3	34.9	39.9
main chain $\langle B\rangle$ (Å^2)	34.1	33.9	38.9
side chain $\langle B\rangle$ (Å^2)	36.2	35.8	41.0
rmsd for angles (deg)	1.5	2.1	2.1
rmsd for bonds (Å)	0.009	0.02	0.02

[a] $R_{sym} = \sum|I_{ij} - \langle I_i\rangle|/\sum I_{ij}$. [b] $R = \sum|F_o - F_c|/\sum|F_o|$.

Table 2: Bond Lengths and Angles for the bsNOS Nitrosyl−Heme Complexes

	Fe−N (NO)	FeNOAngle	Fe−N$^\omega$	Water-N$^\omega$	Water-N(NO)	Water-O(NO)	N$^\omega$-N(NO)	N$^\omega$-O(NO)
bNOS^{2+}+ L-Arg + NO	1.68	132	4.17	2.8	4.0	3.2	2.86	3.10
bNOS^{2+} + NOHA + NO	1.86	126	4.03	2.7	3.9	3.5	2.55	3.00
bNOS^{3+} + NOHA +NO- -I	1.69	161	4.3	3.7	3.9	3.4	3.13	2.87
bNOS^{3+} + NOHA + NO−II	2.29	103	3.87				2.1	3.0

mM dithionite. Crystals were then washed anaerobically and placed in a cryoprotectant containing 4 mM NOC-12 and no reductant or dissolved oxygen. Fe(III)−NO complex crystals were grown in similar conditions but in the absence of dithionite. All crystal and sample handling was carried out in an anaerobic glovebox with all solutions degassed on a Schlenk line. Diffraction data was collected at CHESS F1, F2 beamlines, and NSLS beamlines X6A, X25, and X26 beamlines, respectively. The datasets were reduced and scaled with HKL2000 (*31*). Initial phases were determined using AMoRe (*32*) with the PDB entry 1M7Z of the bsNOS as a molecular replacement model. Refinements were carried out with CNS (*33*) and REFMAC (*34*), and models were built with XFIT (*35*). Structures were refined without energy constraints for bond angles between heme Fe, NO, and NOHA or L-Arg in the complex (Table 1). Multiple starting configurations for the Fe−NO ligation complexes were tested for convergence of geometry. The NO bond length was fixed at 1.15 Å for the Fe(II) complexes and the bent Fe(III)−NO complex and 1.11 Å for the linear Fe(III)−NO complex. The bond angles do not change significantly (less than 2%) when the diatomic ligand is modeled as NO^+, NO, NO^- (bond lengths of 1.11, 1.15, or 1.19 Å, respectively).

RESULTS

Table 2 shows the bond angles and bond distances obtained for the various Fe(II)−NO and Fe(III)−NO complexes. Figure 2A−D shows omit electron density of the bsNOS active sites with NO and substrates bound.

Fe(II)−NO−L-Arg and NOHA Complexes. In the 1.9 Å resolution Fe(II)−NO−L-Arg structure, NO coordinates the heme iron beside the L-Arg guanidinium nitrogen (Figure 2A,B), as observed in the L-Arg NO complex of eNOS (*22*). The NO oxygen [O(NO)] hydrogen bonds to one terminal guanidinium nitrogen and an active-site water molecule that is present above the guanidium group even in the absence of NO. The 1.9 Å resolution structure of the NOHA Fe(II)−NO complex is similar, except that the Fe−N−O bond appears more bent (126° vs 132°). In the NOHA complex, the Fe−N bond length refines slightly longer (1.86 Å) compared to the Fe−N bond length of the L-Arg complex (1.68 Å). Positional refinements were carried out from starting geometries that expanded and contracted the unrestrained Fe−N bond distance by 0.2−0.3 Å. In all cases, the distances refined to within 0.04 Å of the reported values (Table 2). Only with NOHA did the Fe−N distance refine ∼0.14 Å longer than would be expected for a typical heme Fe(II)−NO bond (*36*, *37*). Fixing the Fe(II)−N bond distance to a more typical value of 1.7 Å had little effect on the refined Fe(II)−N−O angle, although at this resolution, the refinement is unlikely to capture a change of <10° in this angle.

Key differences between the L-Arg and NOHA complexes include hydrogen (H)-bonding interactions produced by the NOHA oxime group (C═N−OH). The NOHA hydroxyl oxygen and the main-chain nitrogen of Gly233 are within H-bonding distance, as are the hydroxyl hydrogen and the main-chain carbonyl of Trp234. Additionally, the NOHA N$^\omega$ makes a short H-bond with the proximal nitrogen of NO. Consequently, the N$^\omega$ resides slightly closer to the heme Fe in the NOHA complex, than in the L-Arg complex. Importantly, the interaction between the N(NO) and the NOHA N$^\omega$ nitrogen is shorter (2.55 Å) than between the equivalent guanidinium nitrogen of L-Arg (although the latter is still in hydrogen bonding distance, at 2.86 Å). This interaction, and the nonplanarity of the hydroxy-guanidinum group implies that the hydroxy-guanidinium group protonates on N$^\omega$, as has been found previously in structures of bsNOS (*27*) and mammalian iNOS (*24*) and in agreement with theoretical (*38*,

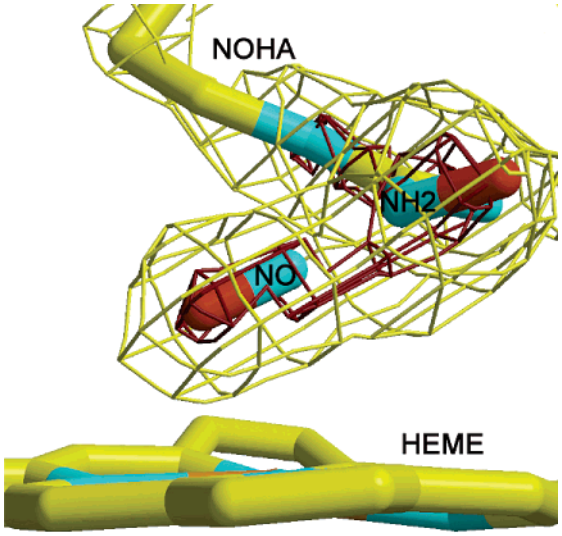

FIGURE 3: An unusually strong interaction between the NOHA N^{ω} and N (NO) indicates at least partial nitrosation of NOHA by Fe(III)−NO. The $F_o - F_c$ electron density, omitting both NOHA and NO from F_c is contoured at 5.5σ (red) and 3σ (yellow).

39) and spectroscopic studies (*40*). Both atoms of NO are in hydrogen-bonding distance to the NOHA N^{ω}, but the distal NO oxygen now resides outside of a typical hydrogen-bonding separation with the active-site water (3.5 Å, Table 2).

Fe(III)−NO−NOHA Complexes. The Fe(III)−NO−NOHA complexes crystallize in a larger unit cell with two molecules in the asymmetric unit (Table 1). The 2.2 Å resolution structure reveals that each molecule has a different Fe(III)−NO conformation (conformations I and II, in Table 2, Figure 2C,D). The first conformation contains a typical linear Fe(III)−NO species. (The more linear geometry of this ligation state compared to the Fe(II)−NO structures indicates that reduction of the heme−nitrosyl center by the X-ray beam does not occur to an appreciable extent in these experiments.) A water molecule resides above the substrate, as in the Fe(II)−NO complexes, but has been displaced toward the mouth of the heme pocket. The second conformation is unusual in that the Fe(III)−NO bond is more bent (100°) when compared to the other Fe(III)−NO or Fe(II)−NO complexes of NOS (*21*). The Fe−N bond length also refines out of range for direct heme ligation (2.29 Å). No obvious water molecule resides above the substrate in conformation II; however, strong electron density near Ile214 could either represent superposition of variable solvent positions, an alternate conformation of the Ile side chain, or an additional NO, which is most consistent with the elongated electron density (Figure 2D). Residues Tyr235, His124, His225, and possibly Ile214 have alternate conformations in this structure. High electron density (5.5σ) in $F_o - F_c$ maps between the NOHA N^{ω} and the N(NO) and a very short interatomic separation (2.1 Å) indicates some covalent bond character between NO and NOHA (Figure 3). Attempts to model this distance as a typical hydrogen-bonding separation (2.7 Å or larger) or a covalent N−N bond (1.3 Å) were both incompatible with the electron density. We thus conclude that the second conformation may represent partial nitrosation of the NOHA N^{ω}.

Attempts to trap a product ternary complex of citrulline with Fe(III)−NO were unsuccessful. Only weak electron density was observed for citrulline in the presence of NO donors, even though NO was not found bound to the heme. In the absence of NO donors, citrulline binds to the active center in a conformation very similar to that of L-Arg and NOHA (Figure 4). In general, lower electron density levels for substrates were found in the presence of NO donor compounds.

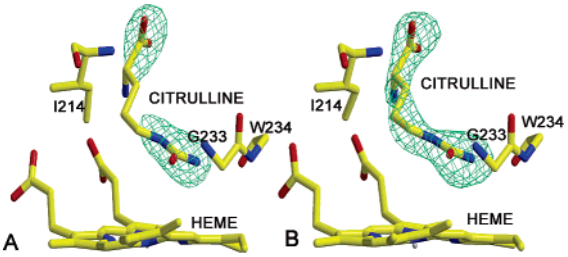

FIGURE 4: Citrulline bound to bsNOS. Presence of NO in solution weakens substrate binding. Citrulline bound to NOS active site in the presence (A) and absence (B) of NO donor compounds (NOC-12). ($F_o - F_c$ omit maps contoured at 3σ.)

DISCUSSION:

The Fe(II)−NO Complexes. The Fe−N−O bond angles for the 1.9 Å resolution Fe(II)−NO complexes with both L-Arg and NOHA bound bsNOS are smaller (132° and 126°) compared to earlier studies on the 2.0 Å resolution Fe(II)−NO complex from the bovine eNOS (161°) (*22*). The more linear bond angle for the eNOS NO complex is similar to the heme−ligand geometry in the 2.4 Å resolution Fe^{3+}−CN complex of murine iNOS (168°) (*23*). At the resolution of our structures, the errors in Fe−NO bond angles are unlikely to exceed ∼15° as larger bond angles do not agree with the experimental electron density and are refined back to ∼130°. Nevertheless, contributions from minor alternate conformations cannot be ruled out at this resolution. Fe−NO bond geometry depends on the electron count of the complex and the environment surrounding the nitrosyl group. In other proteins and model compounds, Fe−NO complexes vary in bond angle from a nearly linear Fe(III)−NO to a severely bent Fe(II)−NO^- (120°), with Fe(II)−NO compounds usually in the range of 130−150° (*36*, *41*, *42*). It is unlikely that the smaller angle in our bsNOS L-Arg complex resulted from additional reduction of the Fe(III)−NO by excess dithionite, as the NO donor compound was introduced after the crystals had been transferred out of the reducing solution. Furthermore, efforts to obtain an Fe−HNO complex using Angeli's salt, which is considered to be a source of HNO/NO^- (*41*), did not yield any heme-bound NO species. Considering that the Fe^{3+}−CN complex of murine iNOS (at 2.4 Å resolution) has nearly the same bond angle as the eNOS nitrosyl−heme compound (168°) could indicate that the latter has some Fe(III)−NO character. However, protein environments are known to influence the geometries of heme ligands (*37*, *43*, *44*). The different Fe−NO geometries of bsNOS and eNOS may also reflect a more constrained heme pocket in bsNOS that results from a Val-to-Ile214 substitution above the distal face of the heme (*27*). One of the features that distinguishes bsNOS from its mammalian counterparts is the tendency of bsNOS to release product NO more slowly from the active center (*30*). This property was shown to correlate with the Val-to-Ile214 substitution in bsNOS (*45*). The additional methylene group of the Ile

side chain directly contacts the distal NO oxygen in both the Fe(II)−NO and Fe(III)−NO bsNOS complexes (with a separation of 3.5−3.8 Å).

Interestingly, the Fe−N bond distance refines ~0.15 Å longer in the NOHA compared to the L-Arg complex. This correlates with bridging electron density between the NOHA N^{ω} atom and the NO(N) indicative of a strong hydrogen-bonding interaction. Density functional theory (DFT) calculations indicate that the Fe−O bond of dioxygen bound to the reduced heme center of mammalian NOS heme will be ~0.15 Å longer than that of Fe−N in the nitrosyl complex (*17*). Thus, the NOS active center may promote a short hydrogen bond between NOHA and the dioxygen proximal oxygen that manifests as a slight distortion in the Fe−N bond length when NO is bound instead of dioxygen. Alternatively, we cannot rule out a minor contribution from another ligation species in the Fe(II)−NO NOHA crystal (perhaps an N-nitrosated NOHA) that when unaccounted for affects the refinement of the Fe−N bond. Nonetheless, difference Fourier electron density maps are essentially flat in this region when the Fe(II)−NO is modeled as a single species with a 1.86 Å Fe−N bond.

The bsNOS Fe(II)−NO−NOHA and L-Arg complexes also differ in solvent interactions within the active center. In both cases, an active-site water molecule forms a hydrogen bond with the NOHA N^{ω}, or its equivalent guanidinium N in L-Arg (Figure 2A,B). However, in the L-Arg complex the O(NO) also hydrogen bonds to this water molecule, but in the NOHA complex, the interatomic separation has increased beyond that of a typical hydrogen bond (Table 2). The NOHA hydroxyl group is in hydrogen-bonding distance with to the main-chain nitrogens of Gly233 and Trp234, whereas the L-Arg terminal guanidinium only hydrogen bonds with bound NO. As a result, the heme Fe is closer to the N^{ω} (4.0 Å) compared to the equivalent nitrogen of L-Arg, which is not hydroxylated (4.2 Å). Similar trends were observed by ENDOR experiments on mammalian neuronal NOS (*40*). The strong interaction between the N(NO) and protonated NOHA N^{ω} directs the O(NO) back, away from the active-site water. This difference may have implications for protonation of peroxo-heme with either L-Arg or NOHA present.

Fe(III)−NO Complexes. The Fe(III)−NO bsNOS complex crystallizes with two molecules per asymmetric unit, which differ primarily in their Fe(III)−NO conformations. Two similar Fe(III)−NO ligation states were found in the Fe(III)−NO complex of nitrophorins, which are small heme proteins designed for NO delivery (*37*, *42*, *46*, *47*). Initial crystal structures of nitrophorin-4 exhibited distorted electron density for the nitrosyl group that was interpreted as two alternate Fe(III)−NO geometries, with one nearly linear Fe−NO bond, and the other severely bent along the porphyrin plane (*46*). However, in later ultra-high-resolution structures of nitrosyl−nitrophorin the severely bent NO was not observed (*37*). The difference between the structures was suggested to derive from photoreduction by the longer wavelength X-ray beam employed in the lower resolution study (*37*). In our bsNOS structure, one Fe(III)−NO bond is close to linear (162°), whereas the other is also unusually bent (100°) with a much longer Fe−NO distance (2.34 Å). Resonance Raman studies of the Fe(III)−NO complexes in iNOS, cytochrome P-450_{cam}, and chloroperoxidase provide

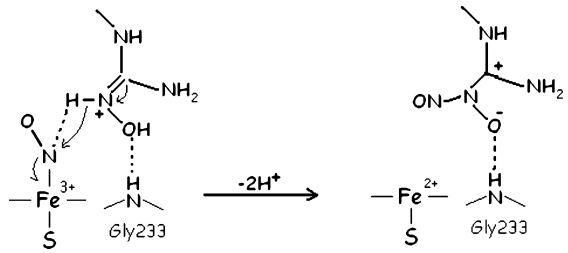

FIGURE 5: Scheme for nitrosation of NOHA by Fe(III)−NO in the bsNOS active center.

support for a nonlinear Fe−NO bending mode (*15*). Photoreduction seems unlikely as a cause for the bent geometry because the crystals were collected with short wavelength radiation (0.979 Å), and we see no such effect with the more reduced Fe(II)−NO complexes. Rather, omit-electron density suggests that the NOHA group is partially nitrosated in the second conformation (Figure 3). Nitrosation of *N*-hydroxyguanidiniums to diazeniumdiolates is known (*48*), and thus N-nitrosation of NOHA by NOS is not unreasonable given the structure of the Fe(III)−NO NOHA complex (Figure 4). Furthermore, ferric nitrosyl−heme species catalyze N-nitrosation reactions of small molecules (*49*) and of cysteine residues in nitrophorin proteins (*42*, *47*); an analogous mechanism may be operative here (Figure 5).

Both mammalian and bacterial NOSs have been implicated in nitrosation and nitration chemistry (*50*, *51*). In one case, the biological function of *Streptomyces* bacterial NOS involves the specific nitration of an indole moiety (*51*). The unusual structure of the Fe(III)NO−NOHA complex indicates that the NOS active center can catalyze nitrosation reactions directly. As mammalian NOSs are often inhibited as the Fe(III)−NO species during turnover (*20*) if small molecules can access the active site, they may be subjected to nitrosation. Given the similarities of their heme centers to NOS, cytochromes P-450 may also have the capacity to nitrosate some of their highly varied substrates.

NO and Substrate Binding. Presence of NO in solution significantly weakens electron density of the L-Arg and NOHA substrates in the active site, compared to structures obtained in the absence of NO donors. The effects of soluble NO were most pronounced for citrulline binding (Figure 4). Thus, a major NO diffusion pathway is likely the same as the substrate access channel. The solvent-accessible surface area of the heme reduces from 20 to 2 $Å^2$ in the presence of L-Arg. The binding of substrates and products will likely effect diffusion of NO and O_2 to and from the heme center.

Mechanistic Implications. Formation of the stable intermediate NOHA breaks the NOS catalytic cycle into two distinct steps, both which are performed by the same active center (*7*, *11*, *52*). The first step, which produces NOHA, likely follows a typical P-450-type monooxygenation reaction. Two net electrons are needed by the heme center for the (i) binding and (ii) activation of oxygen (*52*, *53*). The first electron, which is supplied by the reductase domain, reduces the ferric heme, whereas the second, which comes from H_4B, produces a ferric-peroxo species that may collapse further to a compound I-type species (Figure 1). The second step, which produces NO from NOHA, requires only one exogenous electron; yet to form a reactive catalyst the oxy-heme species must be reduced beyond the Fe(II)−O_2 state. The source of this second electron was originally considered

to derive from NOHA itself (*2*, *3*, *7*, *11*, *54*, *55*); however, recent rapid kinetic experiments point rather to H_4B, as in the first step of the reaction (*56*, *57*). To maintain redox stoichiometry then, the H_3B^+ radical must be reduced in the first step by the reductase domain and in the second step by NOHA-derived products (probably NO^-) (*1*). The favored view of the second step (Figure 1), largely based on chemical analogies, associates a peroxo-species rather than compound I for conversion of NOHA to products (*2*−*11*, *56*, *57*). This then raises the question of how the NOS catalytic center stabilizes two different oxy-heme-species for the two distinct steps, even though the substrates are similar and the delivery of electrons to the catalytic center is essentially identical. No intermediate beyond the ferric-peroxo species, which is common to both steps, has been observed in NOS catalysis (*25*).

A number of groups have suggested that the two reaction steps are distinguished by substrate-controlled delivery of protons and/or hydrogen atoms, to the ferric-heme-superoxy species (*17*, *21*, *25*, *27*, *58*−*60*). Crystallographic and spectroscopic data clearly show that L-Arg can participate in hydrogen-bonding interactions with heme-bound ligands (*15*, *21*). ENDOR spectroscopy of cryo-reduced Fe(II)−O_2 mammalian NOS indicates that the ferric-peroxo group hydrogen bonds with a guanidinium-H_2O network (*25*). On raising temperature, no hydroperoxo intermediate could be isolated before conversion to products. Consistent with this, the eNOS Fe(II)−NO complex reveals a network of hydrogen bonds between the nitrosyl−heme, L-Arg and an active-site water (*21*). These interactions are reproduced by our structure of the bsNOS Fe(II)−NO L-Arg complex, with the exception of a more bent Fe(II)−NO. Notably, in the L-Arg complex, hydrogen-bonding interactions between the guanidinum group and the heme-bound nitrosyl are weaker (longer) than in the NOHA complex, but interaction of the active-center water with the distal nitrosyl oxygen O(NO) is slightly greater (shorter) (Table 2). Importantly, the NOHA N^ω makes a short hydrogen bond to the proximal nitrosyl N(NO), as well as the distal O(NO).

Transfer of a NOHA hydrogen atom was previously thought to provide a proton and electron to the ferric-superoxy species for hydroperoxo formation (*2*, *3*, *7*, *10*, *38*). However, involvement of H_4B in reducing the ferric-superoxy species abrogates the requirement for electron donation from NOHA (*56*, *57*). Furthermore, proton donation to the terminal peroxo-oxygen would be expected to facilitate breakdown of this species to compound I and water. Instead, hydrogen bonding (perhaps even proton donation) to the proximal heme oxygen will stabilize the peroxo-species and thereby promote its reaction with the hydroxy-guanidinium. Less interaction between the active-site water and the distal peroxo-oxygen (as seen in the Fe(II)−NO in NOHA complex) may further stabilize a peroxo species against breakdown. Computational studies of ferric heme-peroxo complexes indicate that protonation of the proximal oxygen prevents O−O cleavage (*61*). We observe stronger bridging electron density between the nitrosyl group and the hydroxy-guanidinium compared to L-Arg, which may also correlate with a shorter hydrogen bond and the lower pK_a of NOHA relative to L-Arg (*62*). Reactivities and structures of NOHA analogues with NOS indicate that the presence of a proton on N^ω is important to promote turnover (*54*), whereas

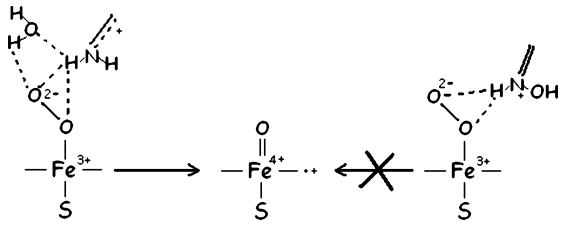

FIGURE 6: Hydrogen bonding by NOHA N^ω to the proximal peroxo-oxygen and reduced hydrogen bonding of H_2O to the distal peroxo oxygen may stabilize a peroxo-heme species in the bsNOS active center during the second step of the reaction.

presence of a proton on the oxime oxygen (N−OH) is not (*3*). Thus, the H_2O-guanidinium network of the L-Arg complex may direct protons toward the distal peroxo-oxygen to facilitate compound I formation, whereas the NOHA N^ω may direct protons toward the proximal (hydro-)peroxo-oxygen to stabilize this species over a high-valent iron-oxo (Figure 6).

The sensitivity of the active-site water structure to substrates and heme ligands suggests that ordered water molecules could reposition when O_2 replaces NO. Such restructuring of active-site water has been demonstrated in crystal structures of cytochromes P-450 ligated to dioxygen (*63*−*65*). In addition to substrate/water hydrogen bonding controlling reactivity of the peroxo-heme species in NOS, protonation of the distal oxy-heme oxygen may also involve of the pterin itself (*59*). This idea stems from the observation that the pterin analogue 4-amino-H_4B cannot support L-Arg oxidation, yet appears to donate an electron to the heme center in the presence of oxygen and both substrates (*59*).

DFT calculations on NOHA bound in the mammalian NOS active center in the presence of Fe(II)−O_2 /Fe(III)−O_2^- support the view that NOHA is most stable when protonated on N^ω (*17*, *39*) (consistent with previous computational studies of NOHA alone (*38*)). The DFT calculations indicate that the N^ω hydrogen bonds with the terminal oxygen atom, whereas the oxime hydroxyl hydrogen bonds with the proximal Fe(II)−O_2 oxygen atom (*17*, *39*). In contrast, our nitrosyl−heme structures suggest that the N^ω hydrogen will interact more strongly with the proximal, rather than the distal, oxygen atom, although it will likely be in hydrogen-bonding distance of both. The N^ω(NOHA)-to-N(NO) interaction appears to distort the Fe−N bond in the direction of what would be expected for an oxygen complex. Thus, these new structures should provide useful starting geometries for further computational studies to test mechanistic issues, including the utility of heme−nitrosyl complexes as mimics for heme-oxy complexes.

DFT calculations of the NOS active center models (*17*) also suggest that there is a prohibitively high cost in energy for forming a tetrahedral intermediate between a nucleophilic heme-bound peroxide and NOHA, a commonly suggested step in conversion to products (*2*, *3*, *7*, *10*, 55). The possible nitrosation of NOHA by Fe(III)−NO in our crystals indicates that the NOHA N^ω is reactive toward electrophilic species. Hydrogen bonding to the proximal peroxo-oxygen will increase the electrophilicity of the distal peroxo-oxygen, which then could add to NOHA and rearrange to generate products (for example, via an oxaziridine-type species; see refs *10* and *24*). Thus, even if peroxo-heme does not operate as a nucleophile in NOS catalysis, it could still be important

for the enzyme to stabilize this intermediate. The short hydrogen-bonding interactions of the protonated NOHA N^{ω} with Fe(II)−NO provides a rationale for such stabilization and further indicates that proton transfer between the NOHA N^{ω} and heme-bound oxygen is a structurally viable pathway during the second step of NOS catalysis.

ACKNOWLEDGMENT

We thank Kanwal Jit Singh and Jawahar Sudhamsu for useful suggestions and help with some figures, and the NSLS and CHESS for access to data collection facilities.

REFERENCES

1. Stuehr, D. J., Santolini, J., Wang, Z.-Q., Wei, C.-C., and Adak, S. (2004) Update on mechanism and catalytic regulation in the NO synthases, *J. Biol. Chem. 279*, 36167−36170.
2. Rosen, G. M., Tsai, P., and Pou, S. (2002) Mechanism of free-radical generation by nitric oxide synthase, *Chem. Rev. 102*, 1191−1199.
3. Huang, H., Hah, J.-M., and Silverman, R. B. (2001) Mechanism of nitric oxide synthase. Evidence that direct hydrogen atom abstraction from the O−H bond of N^{G}-hydroxyarginine is not relevant to the mechanism, *J. Am. Chem. Soc. 123*, 2674−2676.
4. Palmer, R. M. J., Ferrige, A. G., and Moncada, S. (1987) Nitric oxide release accounts for the biological activity of endothelium-derived relaxing factor, *Nature 327*, 524−526.
5. Ignarro, L. J., Buga, G. M., Wood, K. S., Byrns, R. E., and Chaudhuri, G. (1987) Endothelium-derived relaxing factor produced and released from artery and vein is nitric oxide, *Proc. Natl. Acad. Sci. U.S.A. 84*, 9265−9269.
6. Stuehr, D. J., Kwon, N. S., Gross, S. S., Thiel, B. A., Levi, R., and Nathan, C. F. (1989) Synthesis of nitrogen oxides from L-arginine by macrophage cytosol: requirement for inducible and constitutive components, *Biochem. Biophys. Res. Commun. 161*, 420−426.
7. Griffith, O. W., and Stuehr, D. J. (1995) Nitric oxide synthases: properties and catalytic mechanism, *Annu. Rev. Physiol. 57*, 707−736.
8. Klatt, P., Schmidt, K., Lehner, D., Glatter, O., Bachinger, H. P., and Mayer, B. (1995) Structural analysis of porcine brain nitric oxide synthase reveals a role for tetrahydrobiopterin and L-arginine in the formation of an SDS-resistant dimer, *EMBO J. 14*, 3687−3695.
9. Stuehr, D. J., Abu-Soud, H. M., Rousseau, D. L., Feldman, P. L., and Wang, J. (1995) Control of electron transfer in neuronal nitric oxide synthase by calmodulin, substrate, substrate analogs, and nitric oxide, *Adv. Pharmacol 34*, 207−213.
10. Clague, M. J., Wishnok, J. S., and Marletta, M. A. (1997) Formation of N^{δ}-cyanoornithine from N^{G}-hydroxy-L-arginine and hydrogen peroxide by neuronal nitricoxide synthase: implications for mechanism, *Biochemistry 36*, 14465−14473.
11. Marletta, M. A. (1993) Nitric oxide synthase structure and mechanism, *J. Biol. Chem. 268*, 12231−12234.
12. Hurshman, A. R., Krebs, C., Edmondson, D. E., Huynh, B. H., and Marletta, M. A. (1999) Formation of a pterin radical in the reaction of the heme domain of inducible nitric oxide synthase with oxygen, *Biochemistry 38*, 15689−15696.
13. Wei, C.-C., Crane, B. R., and Stuehr, D. J. (2003) Tetrahydrobiopterin radical enzymology, *Chem. Rev. 103*, 2365−2383.
14. Groves, J. T., and Wang, C. C. (2000) Nitric oxide synthase: models and mechanisms, *Curr. Opin. Chem. Biol. 4*, 687−695.
15. Rousseau, D. L., Li, D., Couture, M., and Yeh, S.-R. (2005) Ligand-protein interactions in nitric oxide synthase, *J. Inorg. Biochem 99*, 306−323.
16. Alderton, W. K., Cooper, C. E., and Knowles, R. G. (2001) Nitric oxide synthases: structure, function and inhibition, *Biochem. J 357*, 593−615.
17. Cho, K., and Gauld, J. W. (2005) Second half-reaction of nitric oxide sythase: computational insights into the initial step and key proposed intermediate, *J. Phys. Chem. B. 109*, 23706−23714.
18. Abu-Soud, H. M., Wang, J., Rousseau, D. L., Fukuto, J. M., Ignarro, L. J., and Stuehr, D. J. (1995) Neuronal nitric oxide synthase self-inactivates by forming a ferrous-nitrosyl complex during aerobic catalysis, *J. Biol. Chem. 270*, 22997−23006.
19. Abu-Soud, H. M., Ichimori, K., Nakazawa, H., and Stuehr, D. J. (2001) Regulation of inducible nitric oxide synthase by self-generated NO, *Biochemistry 40*, 6876−6881.
20. Santolini, J., Meade, A. L., and Stuehr, D. J. (2001) Differences in three kinetic parameters underpin the unique catalytic profiles of nitric-oxide synthases I, II, and III, *J. Biol. Chem. 276*, 48887−48898.
21. Li, H., Raman, C. S., Martasek, P., Masters, B. S. S., and Poulos, T. L. (2001) Crystallographic studies on endothelial nitric oxide synthase complexed with nitric oxide and mechanism-based inhibitors, *Biochemistry 40*, 5399−5406.
22. Li, H., Raman, C. S., Martasek, P., Masters, B. S., and Poulos, T. L. (2001) Crystallographic studies on endothelial nitric oxide synthase complexed with nitric oxide and mechanism-based inhibitors, *Biochemistry 40*, 5399−5406.
23. Fedorov, R., Ghosh Dipak, K., and Schlichting, I. (2003) Crystal structures of cyanide complexes of P450cam and the oxygenase domain of inducible nitric oxide synthase-structural models of the short-lived oxygen complexes, *Arch. Biochem. Biophys. 409*, 25−31.
24. Crane, B. R., Arvai, A. S., Ghosh, S., Getzoff, E. D., Stuehr, D. J., and Tainer, J. A. (2000) Structures of the N^{ω}-hydroxy-L-arginine complex of inducible nitric oxide synthase oxygenase dimer with active and inactive pterins, *Biochemistry 39*, 4608−4621.
25. Davydov, R., Ledbetter-Rogers, A., Martasek, P., Larukhin, M., Sono, M., Dawson, J. H., Siler Masters, B. S., and Hoffman, B. M. (2002) EPR and ENDOR characterization of intermediates in the cryoreduced oxy-nitric oxide synthase heme domain with bound L-arginine or N^{G}-hydroxyarginine, *Biochemistry 41*, 10375−10381.
26. Lefevre-Groboillot, D., Frapart, Y., Desbois, A., Zimmermann, J.-L., Boucher, J.-L., Gorren, A. C. F., Mayer, B., Stuehr, D. J., and Mansuy, D. (2003) Two modes of binding of *N*-hydroxyguanidines to NO: evidence for the formation of iron-*N*-hydroxyguanidine complexes and key role of tetrahydrobiopterin in determining the binding mode, *Biochemistry 42*, 3858−3867.
27. Pant, K., Bilwes, A. M., Adak, S., Stuehr, D. J., and Crane, B. R. (2002) Structure of a nitric oxide synthase heme protein from *Bacillus subtilis*, *Biochemistry 41*, 11071−11079.
28. Bird, L. E., Ren, J., Zhang, J., Foxwell, N., Hawkins, A. R., Charles, I. G., and Stammers, D. K. (2002) Crystal structure of SANOS, a bacterial nitric oxide synthase oxygenase protein from *Staphylococcus aureus*, *Structure 10*, 1687−1696.
29. Adak, S., Bilwes Alexandrine, M., Panda, K., Hosfield, D., Aulak Kulwant, S., McDonald John, F., Tainer John, A., Getzoff Elizabeth, D., Crane Brian, R., and Stuehr Dennis, J. (2002) Cloning, expression, and characterization of a nitric oxide synthase protein from Deinococcus radiodurans, *Proc. Natl. Acad. Sci. U.S.A. 99*, 107−112.
30. Adak, S., Aulak, K. S., and Stuehr, D. J. (2002) Direct evidence for nitric oxide production by a nitric-oxide synthase-like protein from *Bacillus subtilis*, *J. Biol. Chem. 277*, 16167−16171.
31. Otwinowski, Z., and Minor, W. (1997) Processing of X-ray diffraction data collected in oscillation mode, *Methods Enzymol. 276*, 307−326.
32. Navaza, J. (1994) AMoRe: an automated package for molecular replacement, *Acta Crystallogr. A A50*, 157−163.
33. Brunger, A. T., Adams, P. D., Clore, G. M., DeLano, W. L., Gros, P., Grosse-Kunstleve, R. W., Jiang, J.-S., Kuszewski, J., Nilges, M., Pannu, N. S., Read, R. J., Rice, L. M., Simonson, T., and Warren, G. L. (1998) Crystallography and NMR system: a new software suite for macromolecular structure determination, *Acta Crystallogr. D D54*, 905−921.
34. Winn, M. D., Isupov, M. N., and Murshudov, G. N. (2001) Use of TLS parameters to model anisotropic displacements in macromolecular refinement, *Acta Crystallogr. D 57*, 122−133.
35. McRee, D. E. (1999) XtalView/Xfit- -A versatile program for manipulating atomic coordinates and electron density, *J. Struct. Biol. 125*, 156−165.
36. Enemark, J. H., and Feltham, R. D. (1974) Stereochemical control of valence. II. Behavior of the $\{MNO\}_n$ [metal mononitrosyl] group in ligand fields, *J. Am. Chem. Soc. 96*, 5002−5004.
37. Roberts, S. A., Weichsel, A., Qiu, Y. Shelnutt, J. A., Walker, F. A., Montfort, W. R. (2001) Ligand-induced heme ruffling and bent NO geometry in ultra-high-resolution structures of nitrophorin 4, *Biochemistry 40*, 11327−11337.
38. Tantillo, D. J., Fukuto, J. M., Hoffman, B. M., Silverman, R. B., Houk, K. N. (2000) Theoretical studies on N^{G}-hydroxy-L-arginine

and dervied radicals: Implications for the mechanism of nitric oxide synthase, *J. Am. Chem. Soc. 122*, 536−537.
39. Cho, K., and Gauld, J. W. (2004) Quantum chemical calculations of the NHA bound nitric oxide synthase active site: O_2 binding and implications for the catalytic mechanism, *J. Am. Chem. Soc*. *126*, 10267−10270.
40. Tierney, D. L., Huang, H., Martasek, P., Masters, B. S. S., Silverman, R. B., and Hoffman, B. M. (1999) ENDOR spectroscopic evidence for the position and structure of N^G-hydroxy-L-arginine bound to holo-neuronal nitric oxide synthase, *Biochemistry 38*, 3704−3710.
41. Farmer Patrick, J., and Sulc, F. (2005) Coordination chemistry of the HNO ligand with hemes and synthetic coordination complexes, *J. Inorg. Biochem 99*, 166−184.
42. Walker, F. A. (2005) Nitric oxide interaction with insect nitrophorins and thoughts on the electronic configuration of the FeNO-(6), *J. Inorg. Biochem. 99*, 216−236.
43. De Angelis F., J., AA., Car, R., and Spiro, T. G. (2005) Quantum chemical evaluation of protein control over heme ligation: CO/O_2 discrimination in myoglobin, *J. Phys. Chem. B. 109*, 3065−3070.
44. Rodgers, K. R., LukaRodgers, G. S., and Barron, J. A. (1996) Structural basis for ligand discrimination and response initiation in the heme-based oxygen sensor FixL, *Biochemistry 35*, 9539−9548.
45. Wang, Z.-Q., Wei, C.-C., Sharma, M., Pant, K., Crane, B. R., and Stuehr Dennis, J. (2004) A conserved Val to Ile switch near the heme pocket of animal and bacterial nitric-oxide synthases helps determine their distinct catalytic profiles, *J. Biol. Chem. 279*, 19018−19025.
46. Weichsel, A., Andersen, J. F., Roberts, S. A., and Montfort, W. R. (2000) Nitric oxide binding to nitrophorin 4 induces complete distal pocket burial, *Nat. Struct. Biol. 7*, 551−554.
47. Weichsel, A., Maes, E. M., Andersen, J. F., Valenzuela, J. G., Shokhireva, T. K., Walker, F. A., and Montfort, W. R. (2005) Heme-assisted S-nitrosation of a proximal thiolate in a nitric oxide transport protein, *Proc. Natl. Acad. U.S.A. 102*, 594−599.
48. Southan, G. J., Srinivasan, A., Keefer, L. K., George, C., and Fales, H. M. (1998) *N*-Nitrosated *N*-hydroxyguanidines are nitric oxide-releasing diazeniumdiolates, *Chem. Commun. 11*, 1191−1192.
49. Bonnett, R. C., Charalambides, A. A., Martin, R. A. (1978) Nitrosation and nitrosylation of haemoproteins and related compounds. Part I. Porphyrins and Metalloporphyrins, *J. Chem. Soc., Perkin Trans.* 974−980.
50. Stamler, J. S., Singel, D. J., and Loscalzo, J. (1992) Biochemistry of nitric oxide and its redox-activated forms, *Science 258*, 1898−1902.
51. Kers, J. A., Wach, M. J., Krasnoff, S. B., Widom, J., Cameron, K. D., Bukhalid, R. A., Gibson, D. M., Crane, B. R., and Loria, R. (2004) Nitration of a peptide phytotoxin by bacterial nitric oxide synthase, *Nature 429*, 79−82.
52. Stuehr, D. J., Kwon, N. S., Nathan, C. F., Griffith, O. W., Feldman, P. L., and Wiseman, J. (1991) N^{ω}-hydroxy-L-arginine is an intermediate in the biosynthesis of nitric oxide from L-arginine, *J. Biol. Chem. 266*, 6259−63.
53. Feldman, P. L., Griffith, O. W., Hong, H., and Stuehr, D. J. (1993) Irreversible inactivation of macrophage and brain nitric oxide synthase by L-N^{ω}-methylarginine requires NADPH-dependent hydroxylation, *J. Med. Chem. 36*, 491−496.
54. Li, H., Shimizu, H., Flinspach, M., Jamal, J., Yang, W., Xian, M., Cai, T., Wen Edward, Z., Jia, Q., Wang Peng, G., and Poulos Thomas, L. (2002) The novel binding mode of *N*-alkyl-*N*′-hydroxyguanidine to neuronal nitric oxide synthase provides mechanistic insights into NO biosynthesis, *Biochemistry 41*, 13868−13875.
55. Korth, H. G., Sustmann, R., Thater, C., Butler, A. R., and Ingold, K. U. (1994) On the mechanism of the nitric oxide synthase-catalyzed conversion of N^{ω}-hydroxyl-L-arginine to citrulline and nitric oxide, *J. Biol. Chem. 269*, 17776−17779.
56. Wei, C.-C., Wang, Z.-Q., Hemann, C., Hille, R., and Stuehr, D. J. (2003) A tetrahydrobiopterin radical forms and then becomes reduced during N^{ω}-hydroxyarginine oxidation by nitric-oxide synthase, *J. Biol. Chem. 278*, 46668−46673.
57. Sorlie, M., Gorren, A. C. F., Marchal, S., Shimizu, T., Lange, R., Andersson, K. K., and Mayer, B. (2003) Single-turnover of nitric-oxide synthase in the presence of 4-amino-tetrahydrobiopterin: proposed role for tetrahydrobiopterin as a proton donor, *J. Biol. Chem. 278*, 48602−48610.
58. Crane, B. R., Arvai, A. S., Gachhhui, R., Wu, C., Ghosh, D. K., Getzoff, E. D., Steuhr, D. J., and Tainer, J. A. (1997) The structure of nitric oxide synthase oxygenase domain and inhibitor complexes, *Science 278*, 425−431.
59. Marchal, S., Gorren, A. C. F., Sorlie, M., Andersson, K. K., Mayer, B., and Lange, R. (2004) Evidence of two distinct oxygen complexes of reduced endothelial nitric oxide synthase, *J. Biol. Chem. 279*, 19824−19831.
60. Stuehr Dennis, J., Santolini, J., Wang, Z.-Q., Wei, C.-C., and Adak, S. (2004) Update on mechanism and catalytic regulation in the NO synthases, *J. Biol. Chem. 279*, 36167−36170.
61. Harris, D. L., and Loew, G. (1998) Theoretical investigation of the proton assisted pathway to formation of cytochrome P-450 compound I, *J. Am. Chem. Soc. 120*, 8941−8948.
62. Lefevre-Groboillot, D., Dijols, S., Boucher, J. L., Mahy, J. P., Ricoux, R., Desbois, A., Zimmermann, J. L., and Mansuy, D. (2001) *N*-hydroxyguanidines as new heme ligands: UV−visible, EPR, and resonance Raman studies of the interaction of various compounds bearing a C═NOH function with microperoxidase-8, *Biochemistry 40*, 9909−9917.
63. Nagano, S., Cupp-Vickery, J. R., and Poulos, T. L. (2005) Crystal structures of the ferrous dioxygen complex of wild-type cytochrome P450eryF and its mutants, A245S and A245T: investigation of the proton-transfer system in P450eryF, *J. Biol. Chem. 280*, 22102−22107.
64. Nagano, S., and Poulos, T. L. (2005) Crystallographic study on the dioxygen complex of wild-type and mutant cytochrome P450cam. Implications for the dioxygen activation mechanism, *J. Biol.* Chem. *280*, 31659−31663.
65. Schlichting, I., Berendzen, J., Chu, K., Stock, A. M., Maves, S. A., Benson, D. E., Sweet, R. M., Ringe, D., Petsko, G. A., and Sligar, S. G. (2000) The catalytic pathway of cytochrome P450cam at atomic resolution, *Science 287*, 1615−1622.

BI0518848